DV–Xα Calculations, UV–PE Spectra, and Redox Properties of Nitrosyl-Bridged Binuclear Cobalt Complexes

Giuseppe Pilloni,*[1a] Sandro Zecchin,[1b] Maurizio Casarin,[1c] and Gaetano Granozzi*[1a]

Dipartimento di Chimica Inorganica, Metallorganica ed Analitica, University of Padova, Istituto di Polarografia ed Elettrochimica Preparativa del CNR, and Istituto di Chimica e Tecnologia dei Radioelementi del CNR, Padova, Italy

Received June 30, 1986

The electronic structure of two cobalt dimers containing bridging nitrosyl groups, $(\mu\text{-NO})_2[Co(\eta^5\text{-}C_5H_5)]_2$ (I) and $(\mu\text{-NO})(\mu\text{-CO})[Co(\eta^5\text{-}C_5H_5)]_2$ (II), has been investigated by vapor-phase UV photoelectron (PE) spectroscopy and electrochemical techniques. The information obtained by the two experimental approaches was fit together in a unique bonding picture by DV–Xα quantum mechanical calculations. The UV–PE spectrum of I is consistent with a bent $(\mu\text{-NO})_2Co_2$ core in the vapor phase, in contrast with the planar core observed in the solid state. The theoretical calculations predict a direct Co–Co interaction for the bent geometry, at variance with the planar one where no charge accumulation between the metal atoms is computed. The bonding scheme emerging from the calculations is consistent with the redox behavior of both I and II. Both complexes were found to undergo reversible one-electron-transfer processes revealing the existence of the redox couples $I^{0/1-}$, $I^{1+/0}$, $I^{2+/1+}$, $II^{0/1-}$, and $II^{1+/0}$. Except reduction of II, either removal or addition of electrons resulted, however, in bridge splitting follow-up reaction. Bridge cleavage in I^- is a consequence of the filling of the strongly antibonding Co–NO LUMO, while in I^{2+} it arises from the large decrease of the $d_\pi(Co) \rightarrow \pi^*(NO)$ back-bonding owing to the high positive charge on the metal atoms. The observed reaction mode of II^+ into 15-electron $[CoCp(CO)]^+$ and 17-electron CoCp(NO) fragments has been tentatively attributed to a charge polarization effect consequent to the presence of two different bridging groups. Otherwise, kinetic factors were found to merely rationalize the unstability of intermediate I^+.

Introduction

The electronic structure of polynuclear organometallic molecules has been the object of several investigations involving theoretical and spectroscopical approaches. The main goal of these studies is the explanation of the nature of the multicentered metal–ligand interactions that are expected to be similar to those present in surface complexes formed on catalytic metal surfaces.[2]

In the case of ligand-bridged binuclear systems, the main question to be answered is related to the real existence of direct metal–metal interactions that are usually predicted employing the qualitative EAN rule. Recent evidence on carbonyl-bridged dimers, however, has proposed a rather different picture where the electron pairing between the two metals occurs via delocalized multicentered bonds representing concerted back-donation interactions to bridging carbonyl $2\pi^*$ levels.[3]

In order to verify if this bonding picture is valid also for nitrosyl-bridged dimers, two cobalt binuclear complexes, namely, $(\mu\text{-NO})_2[Co(\eta^5\text{-}C_5H_5)]_2$ (I) and $(\mu\text{-NO})(\mu\text{-CO})[Co(\eta^5\text{-}C_5H_5)]_2$ (II) (hereafter Cp = $\eta^5\text{-}C_5H_5$), have been thoroughly investigated.

Two different approaches have been employed: (i) the vapor-phase ultraviolet photoelectron (UV–PE) spectroscopy, capable of providing directly an energy map of one-electron occupied molecular orbitals (MOs), and (ii) electrochemical techniques, which can give indirect information on the frontier MOs by examining the chemical behavior of the oxidation–reduction products. Moreover, theoretical calculations on I, based on the *first-principle* discrete variational (DV) Xα method, have been used to fit together the information obtained by the two experimental approaches in an unique bonding picture.

The redox properties of carbonyl- and nitrosyl-bridged metal cyclopentadienyl dimers have received considerable attention.[4] In particular, previous cyclic voltammetric studies on I have shown the occurrence of reversible oxidation–reduction reactions revealing the existence of the three-membered redox series I^z (z = 0 to 2+).[5] Notably I^+ has been isolated and stereochemically characterized by Wochner et al.[6] from IR measurements in solution and X-ray diffraction study in the solid state as the $[BF_4]^-$ salt. Conversely, the electrochemical reduction of I has been reported to be an irreversible process involving nitrosyl bridge cleavage,[7] since the formation of $[CoCp(NO)]^-$ (III) by the reaction of the dimer with sodium amalgam was observed.[8] This redox behavior of I is opposite to that exhibited under similar conditions by its isostructural nitrosyl–carbonyl analogue II, which was found to retain its bimetallic nature upon reduction while probably undergoing scission upon oxidation.[7]

We report here a comprehensive investigation, including bulk electrolyses at controlled potentials, on the electrochemical behavior of I and II with the basic objective of gaining further insight into the main transformations occurring on these dimers upon either removal or addition

(1) (a) University of Padova. (b) IPELP CNR of Padova. (c) ICTR CNR of Padova.

(2) (a) Ugo, R. *Catal. Rev.* **1975**, *11*, 225. (b) Muetterties, E. L.; Rhodin, T. N.; Band, E.; Brucker, C. F.; Pretzer, W. R. *Chem. Rev.* **1979**, *79*, 91.

(3) (a) Mitscher, A.; Rees, B.; Lehmann, M. S. *J. Am. Chem. Soc.* **1978**, *100*, 3390. (b) Bénard, M. *J. Am. Chem. Soc.* **1978**, *100*, 7740. (c) Bénard, M. *Inorg. Chem.* **1979**, *18*, 2782. (d) Granozzi, G.; Tondello, E.; Bénard, M.; Fragalà, I. *J. Organomet. Chem.* **1980**, *194*, 83. (e) Granozzi, G.; Casarin, M.; Ajò, D.; Osella, D. *J. Chem. Soc., Dalton Trans.* **1982**, 2047. (f) Bottomley, F. *Inorg. Chem.* **1983**, *22*, 2656.

(4) Representative papers are: (a) Ferguson, J. A.; Meyer, T. J. *Inorg. Chem.* **1971**, *10*, 1025. (b) *Ibid.* **1972**, *11*, 631. (c) Schore, N. E.; Ilenda, C. S.; Bergman, R. G. *J. Am. Chem. Soc.* **1976**, *98*, 256. (d) *Ibid.* **1977**, *99*, 1781. (e) Clamp, S.; Connelly, N. G.; Payne, J. D. *J. Chem. Soc., Chem. Commun.* **1981**, 897. (f) Seidler, M. D.; Bergman, R. G. *Organometallics* **1983**, *2*, 1897. (g) Davies, S. G.; Simpson, S. J.; Parker, V. D. *J. Chem. Soc., Chem. Commun.* **1984**, 352. (h) Legzdins, P.; Wassink, B. *Organometallics* **1984**, *3*, 1811 and references cited therein.

(5) Connelly, N. G.; Payne, J. D.; Geiger, W. E. *J. Chem. Soc., Dalton Trans.* **1983**, 295.

(6) Wochner, F.; Keller, E.; Brintzinger, H. H. *J. Organomet. Chem.* **1982**, *236*, 267.

(7) Bernal, I.; Korp, J. D.; Reisner, G. M.; Herrmann, W. A. *J. Organomet. Chem.* **1977**, *139*, 321.

(8) Weiner, W. P.; White, M. A.; Bergman, R. G. *J. Am. Chem. Soc.* **1981**, *103*, 3612.

0276-7333/87/2306-0597$01.50/0

of electrons as well as in obtaining a better understanding of the kinetic and thermodynamic factors responsible for the stability of both oxidized and reduced species.

Experimental Section

Materials. The $(\mu\text{-NO})_2[\text{CoCp}]_2$ (I) and $(\mu\text{-NO})(\mu\text{-CO})[\text{CoCp}]_2$ (II) complexes were prepared and purified by published procedures.[9] Reagent grade 1,2-dimethoxyethane (DME) was purified by refluxing over $LiAlH_4$; it was stored over $LiAlH_4$ until needed and then carefully distilled under nitrogen. Tetrabutylammonium perchlorate (TBAP) was crystallized twice from ethyl acetate and dried under vacuum at 60 °C. All other chemicals employed were of reagent grade quality and were used without further purification. Argon (99.999%), rendered oxygen free by passage over reduced copper at 450 °C, was used.

Instrumentation. Infrared (IR) spectra were recorded with a Perkin-Elmer Model 682 spectrometer. Solution spectra were measured with compensation in 0.05-cm CaF_2 liquid cells. Electronic spectra were run on a Cary Model 17 D spectrophotometer. ESR spectra were taken on a Brucker model ER 100D X-band spectrometer. He I excited PE spectra in vapor phase were obtained on a Perkin-Elmer PS-18 spectrometer. The ionization energy (IE) scale was calibrated by reference to peaks due to admitted inert gases (Xe–Ar) and to the He $1s^{-1}$ self-ionization. A heated inlet probe system was adopted at 110 °C. The apparatus used for voltammetry consisted of an Amel Model 551 potentiostat modulated by an Amel model 566 function generator while the recording device was either a Hewlett-Packard model 7040 A XY recorder or a Gould Advance model OS 4100 digital storage oscilloscope with analogue output for XY recorders, depending on the scale rate employed. Controlled potential electrolyses were carried out with an Amel model 552 potentiostat, and the associated coulometer was an Amel model 731 digital integrator.

Cell and Electrodes. All experiments were performed on anhydrous, deoxygenated DME solutions with 0.2 M TBAP as the supporting electrolyte, using a conventional three-electrode liquid-jacketed cell. In the voltammetric tests the working electrode was a planar platinum microelectrode (ca. 0.3 mm^2) surrounded by a platinum spiral counter electrode. The potential of the working electrode was probed by a Lugging capillary-reference electrode compartment whose position was made adjustable by mounting it on a syring barrel. Compensation of iR drop was further achieved by positive feedback. In the bulk electrolyses the working electrode was a platinum gauze (ca. 100 cm^2) and the counter electrode was external, the connection being made through an appropriate salt bridge. In all cases a silver/0.1 M silver perchlorate electrode in acetonitrile, separated from the test solution by 0.2M TBAP solution in DME sandwiched between two fritted disks, was used as the reference electrode (E = –0.05 V vs. ferricinium/ferrocene in DME, 0.2 M TBAP).[10] All potentials are referred to the ferricinium/ferrocene couple. Unless otherwise stated, cyclic voltammograms (CV) were run at 0.2 V s^{-1} and voltammograms with renewal of the diffusion layer (RDLV)[11] at a renewal time of 2.0 s.

Calculations. Hartree–Fock–Slater (HFS) discrete variational (DV–Xα) calculations[12] were performed on a VAX-11/750 computer. Numerical atomic orbitals obtained for the neutral atoms (through 4p for Co and 2p for C, N, and O) were used as basis functions. Due to the size of the investigated systems, orbitals 1s–3p (Co) and 1s on C, N, and O were treated as the frozen core in the molecular calculations. The molecular electronic density was approximated with an s-wave expansion, and the HFS equations were solved by a self-consistent charge (SCC) procedure[12] using the Gaspar–Kohn–Sham value[13] for the exchange scaling parameter. Atomic orbital populations were computed by using the Mulliken analysis.[14] To evaluate the magnitude of electronic relaxation associated with the removal of one electron from the various ground-state MOs, IE calculations were carried out by using Slater's transition-state formalism (TSIE).[15] Two sets of calculations have been run on I, assuming either a planar or a bent form for the $(\mu\text{-NO})_2Co_2$ core (see Figure 1). The geometry of the planar conformation (C_{2h}) has been obtained from the solid-state structural determination.[7] The bent one (C_{2v}) has been inferred from the structural data on the isoelectronic $(\mu\text{-CO})_2[\text{NiCp}]_2$.[16a]

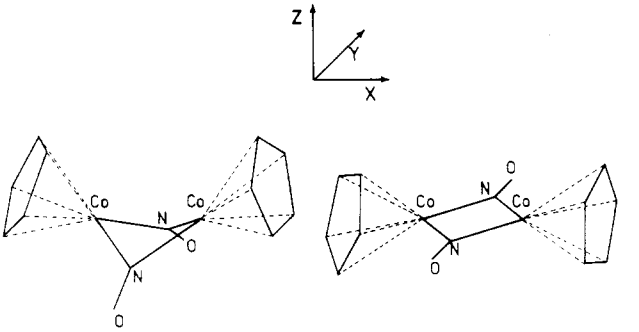

Figure 1. Schematic view of the bent and planar geometries of $(\mu\text{-NO})_2[\text{Co}(\eta^5\text{-}C_5H_5)]_2$ (I) with the axis system adopted in the calculations.

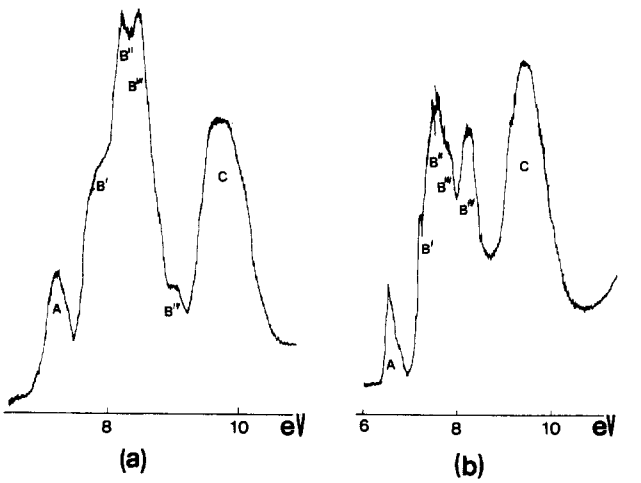

Figure 2. He I excited vapor-phase PE spectra of $(\mu\text{-NO})_2[\text{Co}(\eta^5\text{-}C_5H_5)]_2$ (a) and $(\mu\text{-NO})(\mu\text{-CO})\text{-}[\text{Co}(\eta^5\text{-}C_5H_5)]_2$ (b).

Table I. IR and Vis-Near-IR Data for Binuclear Co Complexes in 1,2-Dimethoxyethane, 0.2 M TBAP Solution

complex	ν_{NO}/cm^{-1}	ν_{CO}/cm^{-1}	λ_{max}/nm^a
$[\text{CoCp(NO)}]_2$ (I)	1595 (m) 1541 (vs)		475 (sh), 600 (sh)
$[\text{CoCp(NO)}]_2^{\cdot+}$ (I^+)	1617 (vs)		535 (ϵ 4500), 990 (ϵ 400)
$[Co_2Cp_2(CO)(NO)]^{\cdot}$ (II)	1555 (vs)	1838 (vs)	457 (ϵ 3800), 1000 (ϵ 180)
$[Co_2Cp_2(CO)(NO)]^-$ (II^-)	1436 (vs)	1735 (vs)	no max

[a] ϵ in $dm^3\ mol^{-1}\ cm^{-1}$.

Results and Discussion

UV–PE and Theoretical Results. Following the usual EAN formalism, complex I should have a formal bond

(9) (a) Brunner, H. *J. Organomet. Chem.* **1968**, *12*, 517. (b) Herrmann, W. A.; Bernal, I. *Angew. Chem.* **1977**, *89*, 186.

(10) Under the same conditions the peak separation for ferrocene oxidation is 60 mV at 25 °C for a scan rate of 200 mV s^{-1}.

(11) Schiavon, G.; Mazzochin, G. A.; Bombi, G. G. *J. Electroanal. Chem.* **1971**, *29*, 401.

(12) (a) Averill, F. W.; Ellis, D. E. *J. Chem. Phys.* **1973**, *59*, 6411. (b) Rosen, A.; Ellis, D. E.; Adachi, H.; Averill, F. W. *J. Chem. Phys.* **1976**, *65*, 3629 and references therein. (c) Trogler, W. C.; Ellis, D. E.; Berkowitz, J. *J. Am. Chem. Soc.* **1979**, *101*, 5896.

(13) (a) Kohn, W.; Sham, L. J. *Phys. Rev.* **1965**, *140*, A1133. (b) Gaspar, R. *Acta Phys. Acad. Sci. Hung.* **1954**, *3*, 263.

(14) Mulliken, R. S. *J. Chem. Phys.* **1955**, *23*, 1833.

(15) Slater, J. C. *Quantum Theory of Molecules and Solids. The Self-Consistent Field For Molecules and Solids*; McGraw-Hill: New York, 1974; Vol. 4.

Table II. DV-Xα Results for Bent $(\mu\text{-NO})_2[Co(\eta^5\text{-}C_5H_5)]_2$ (I)

MO	eigenvalue[a]	TSIE[a]	compn, % 2 Co	2 NO	2 Cp	character[c]
$11b_2$ (LUMO)	−2.552	5.090[b]	15	75	10	π*NO, Co–NO ab
$12b_1$ (HOMO)	−4.234	6.826	72	12	16	Co–Co ab
$11b_1$	−4.715	7.493	86	3	11	Co–Co ab
$8a_2$	−4.723	7.250	63	17	20	Co–Co ab
$15a_1$	−5.168	7.733	71	13	16	Co–Co b
$7a_2$	−5.364	7.952	51	38	11	Co–Co ab
$10b_1$	−5.450	8.093	47	44	9	Co–Co ab; Co–NO b
$10b_2$	−5.637	8.336	79	15	6	Co–Co b
$14a_1$	−5.688	8.342	79	10	11	Co–Co b
$13a_1$	−6.107	8.566	57	24	19	Co–Co b
$9b_1$	−7.027	9.261	21	0	79	Co–Cp π bonding
$9b_2$	−7.028	9.296	15	3	82	
$6a_2$	−7.200	9.480	26	3	71	
$12a_1$	−7.243	9.500	34	3	63	

[a] In eV. [b] Extimated from TS calculation on HOMO. [c] b = bonding; ab = antibonding.

order of 1 between the two d^9 Co atoms (assuming NO^+). Even though it shows a planar $(\mu\text{-NO})_2Co_2$ core in the solid state,[17] the presence of two nitrosyl stretching frequencies in its solution IR spectrum (see Table I) is indicative of a bent geometry (see Figure 1). The high flexibility of the $(\mu\text{-}L_2)M_2$ core (d^9–d^9 and d^8–d^9 metals; L = CO, NO) is well-documented both experimentally[16] and theoretically.[17] Actually, conformational changes have been observed on passing from solid to either solution or vapor phase.[16] Due to the lack of any structural evidence in the vapor phase for I, we decided to perform distinct calculations assuming a planar and a bent geometry. The comparison between experimental UV–PE data and theoretical results (see below) gives strong support to the presence in the vapor phase of a bent geometry.

The low IE region (6–11 eV) of the He I excited PE spectrum of I is reported in Figure 2a, where bands have been labeled alphabetically. The higher IE region, consisting of a broad and ill-resolved structure mainly due to inner π and σ Cp and NO levels, is not reported because no information can be extracted from it. In the report region three bands are present (A, 7.11 eV; B, ca. 8 eV; C, 9.5 eV), band B showing four resolved components (B^I, 7.67 eV; B^{II}, 7.98 eV; B^{III}, 8.23 eV; B^{IV}, 8.89 eV). All the bands are shifted toward higher IEs with respect to the corresponding ones of the previously reported pentamethylated analogue,[18] in tune with the expected perturbations induced by the methyl substitutions. It is noteworthy, however, that the assignments of the pentamethylated literature PE spectrum[18] have been carried out by assuming a planar core in the vapor phase.

The UV–PE data on related bridged dimers[3d,e,18,19] suggests that the reported IE region should contain at least 13 different ionizations; four of them are related to MOs representing Co–Cp π-bonding interactions while the remaining come from MOs with a predominant contribution of 3d Co AOs, hereafter referenced as metal-based orbitals.

Following the Hoffmann's suggestion, the M–Cp fragment "remembers its octahedral parentage"[17,21] so that its metal-based orbitals can be labeled as e_g- and t_{2g}-like. The higher lying e_g set (two MOs) accounts for the M–Cp π-antibonding interaction while the t_{2g}-like one (three MOs) consists of strongly metal-localized orbitals. When two M–Cp fragments are allowed to interact to give rise to the M_2–Cp_2 unit, bonding and antibonding combinations (with respect to M–M interaction) of both sets are obtained.

In the previous study on the $(\mu\text{-CO})_2[NiCp]_2$ complex[3e] (showing a planar core in the vapor phase[20] and isoelectronic with I), the metal-based orbitals were actually split in two distinct groups that can be directly related to the above described e_g- and t_{2g}-like sets. Among the four e_g-like MOs, three of them were occupied and they accounted for M–Cp antibonding, M–CO back-bonding, and M–M π interactions.

In the PE spectrum of I the splitting between the e_g- and t_{2g}-like sets is reduced by two concurrent reasons: (i) the expected smaller crystal field splitting of the Co–Cp fragment with respect to the Ni–Cp one, (ii) the higher π acidity of NO with respect to CO which allows a stronger interaction between NO 2π* MOs and e_g-like components. As a consequence, we expect that e_g- and t_{2g}-like ionizations will strongly overlap.

In Figure 3 the experimental IEs of I have been compared with the theoretical TSIEs computed assuming a planar or a bent $(\mu\text{-NO})_2Co_2$ core. The most relevant difference between the two sets of TSIEs is the energy position of the HOMO, which is strongly stabilized in the bent form, and gives rise to a definitely better agreement with experimental IEs. This evidence strongly supports the existence of a bent geometry in the vapor phase, as found in solution (Table I). Thus, only the charge density analysis of the DV–Xα outermost MOs obtained for the bent conformer is reported (see Table II).

Let us first consider the total electron density map in the *XY* plane (Figure 4a). A significative charge accumulation between the two Co atoms is clearly evident, supporting the existence of a direct Co–Co bond. Interestingly, the inspection of relative *XZ* slice (Figure 4b) points out the nonbent nature of such a bond. The presence of this interaction is a consequence of the bent geometry, as clearly demonstrated by the comparison with Figure 5 where the total electron density in the $(\mu\text{-NO})_2Co_2$ plane does not show any charge accumulation between the Co atoms.

Going on with the analysis of the outermost MOs, four of them ($13a_1$, $14a_1$, $10b_2$, $15a_1$) are metal–metal bonding

(16) (a) Byers, L. R.; Dahl, L. F. *Inorg. Chem.* **1980**, *19*, 680. (b) Cirjak, L. M.; Ginsburg, R. E.; Dahl, L. F. *Inorg. Chem.* **1982**, *21*, 940.
(17) Pinhas, A. R.; Hoffmann, R. *Inorg. Chem.* **1979**, *18*, 654.
(18) Dudeney, N.; Green, J. C.; Kirchner, O. N.; Smallwood, F. St. J. *J. Chem. Soc., Dalton Trans.* **1984**, 1883.
(19) Granozzi, G.; Tondello, E.; Ajò, D.; Faraone, F. *J. Organomet. Chem.* **1982**, *240*, 191.
(20) Miller, J. R. *Adv. Inorg. Chem. Radiochem.* **1962**, *4*, 133.
(21) (a) Elian, M.; Hoffmann, R. *Inorg. Chem.* **1975**, *14*, 1058. (b) Elian, M.; Chen, M. M. L.; Mingos, M. P.; Hoffmann, R. *Inorg. Chem.* **1976**, *15*, 1148.
(22) Alberts, G. S.; Shain, I. *Anal. Chem.* **1963**, *35*, 1859.

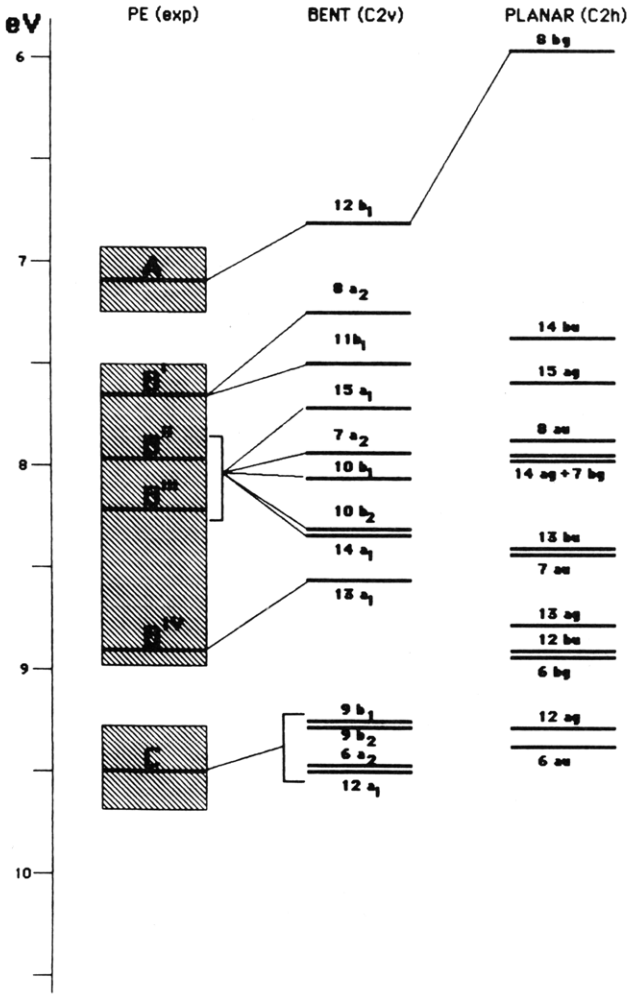

Figure 3. Correlation diagram between experimental IEs and DV–Xα theoretical TSIEs for $(\mu\text{-NO})_2[\text{Co}(\eta^5\text{-}C_5H_5)]_2$ (I) with a bent and planar core.

whereas $10b_1$, $7a_2$, $8a_2$, $11b_1$, and $12b_1$ MOs are antibonding with respect to the same interaction (Table II). The inconsistency between the presence of a direct metal–metal bond (see Figure 4) and the higher number of Co–Co antibonding MOs with respect to bonding ones is only apparent because the contribution to the overall Co–Co bond order is different for each MO, according to their degree of localization.

The bridging nitrosyls contribute to the MOs reported in Table II mainly through their $2\pi^*$ sets. Some small contribution from 5σ inner levels is symmetry-allowed only in a_1- and b_2-type MOs. In order to obtain a better description of the nature of some selected MOs, relative contour plots (CPs) in XY and XZ planes are reported in Figure 6.

The $12b_1$ HOMO (whose ionization is to be related to band A of Figure 2) represents (see Figure 6) Co–Co and Co–Cp π-antibonding interactions mainly localized in the XZ plane, in agreement with Hückel-type calculations on the isoelectronic $[\text{CoCp(CO)}]_2^{2-}$[17] and ESR and X-ray experimental evidence on $[\text{CoCp(CO)}]_2^-$.[4d,16] The aforesaid stabilization of this MO with respect to the planar geometry is mainly due to the reduced Co–Cp antibonding character (the contribution to the HOMO from the Cp rings passes from 30 to 16%) and not to the bridging nitrosyl contribution, which is scarce and Co–N antibonding in character. Among the subsequent MOs, the $10b_1$ one has the largest Co–NO bonding character; this MO is reminiscent of that describing the delocalized

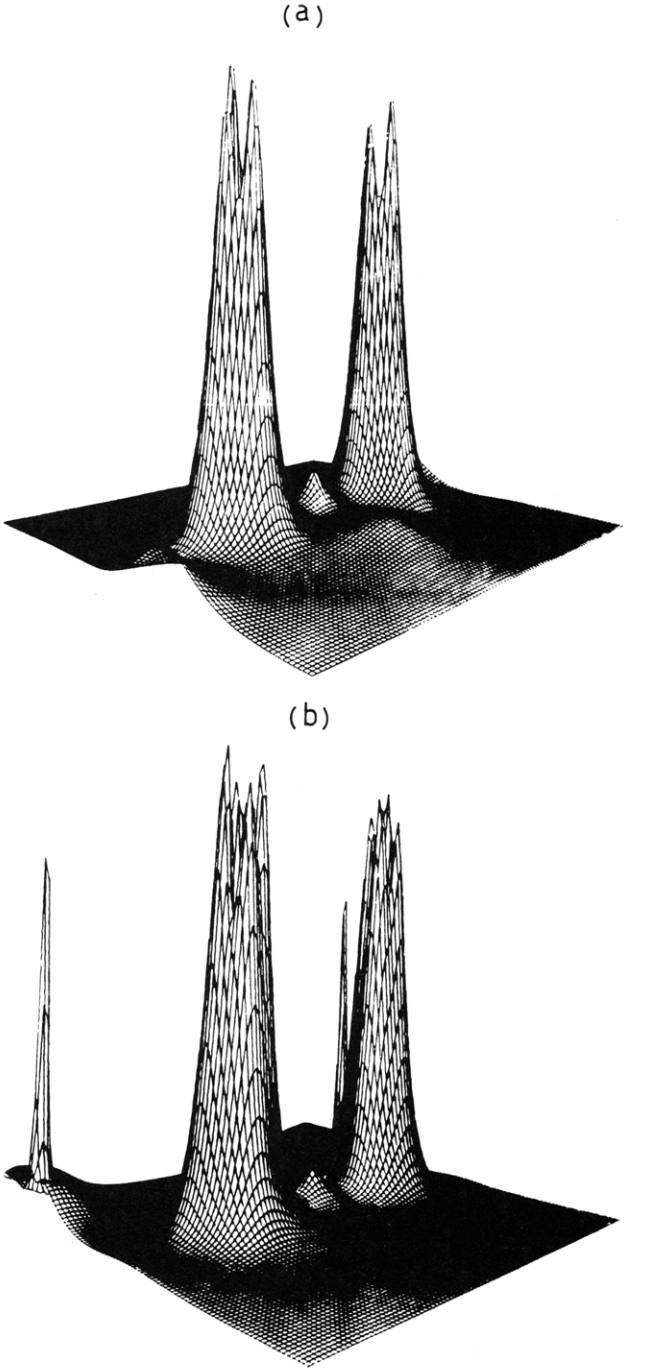

Figure 4. DV–Xα total electron density map in the XY plane (a) and XZ plane (b) of bent $(\mu\text{-NO})_2[\text{Co}(\eta^5\text{-}C_5H_5)]_2$ (I).

multicentered bond responsible for the electron pairing between the metal atoms found in similar $(\mu\text{-CO})_2M_2$ systems.[3] At variance with the previous cases, the ionization from this MO is not the lowest lying IE event (see below) because of the higher π acceptor capability of NO vs. CO ligand.

The band B is associated as a whole to eight ionizations (Figure 3); intensity arguments suggest to assign B^I to the ionization from two MOs ($8a_2$ and $11b_1$), the B^{II}–B^{III} envelope to five components ($15a_1$, $7a_2$, $10b_1$, $10b_2$, and $14a_1$) and the low-intensity shoulder B^{IV} to the ionization from the $13a_1$ MO. Finally, band C contains the ionizations from the four Co–Cp π-bonding orbitals ($9b_1$, $9b_2$, $6a_2$, $12a_1$).

The CP relative to the LUMO of I is reported in Figure 7. It is of relevance to the forthcoming analysis of the electrochemical data to point out that this MO is strongly Co–NO antibonding, so that we can anticipate a strong

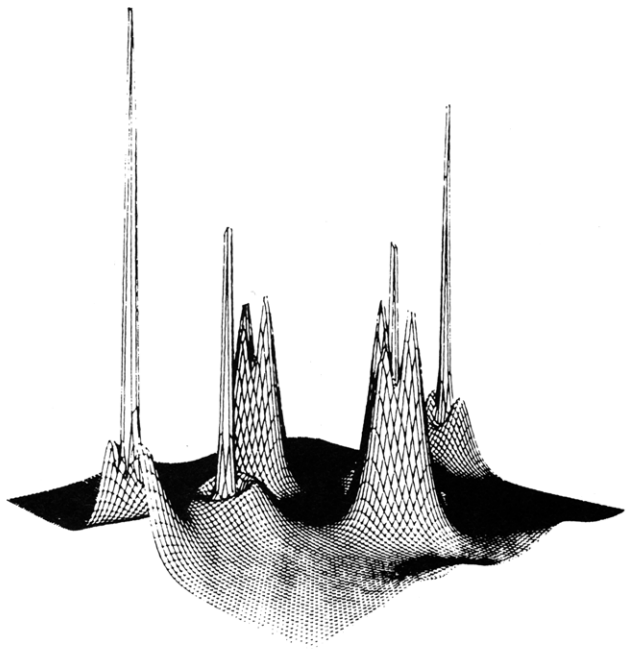

Figure 5. DV–Xα total electron density map in the $(\mu\text{-NO})_2Co_2$ plane of planar $(\mu\text{-NO})_2[Co(\eta^5\text{-}C_5H_5)]_2$ (I).

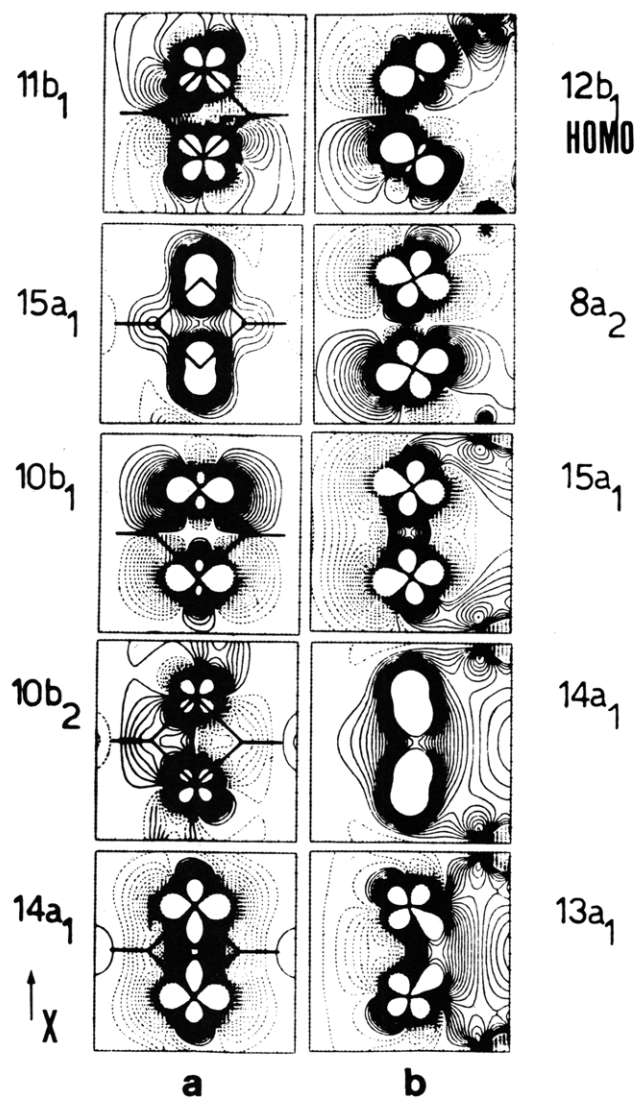

Figure 6. DV–Xα contour plots of selected MOs of bent $(\mu\text{-NO})_2[Co(\eta^5\text{-}C_5H_5)]_2$ (I) in the XY (a) and XZ (b) planes. The interval between successive contour levels is 0.0337 $e^{1/2}/Å^{3/2}$.

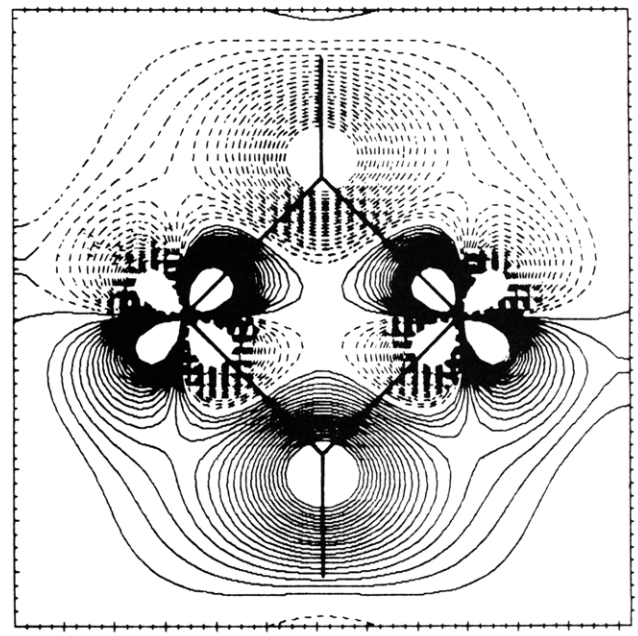

LUMO

Figure 7. DV–Xα contour plot of the $11b_2$ LUMO of bent $(\mu\text{-NO})_2[Co(\eta^5\text{-}C_5H_5)]_2$ (I) in the XY plane. The interval between successive contour levels is 0.0337 $e^{1/2}/Å^{3/2}$.

destabilization of the dimeric structure upon its filling.

The He I PE spectrum of II (an open-shell molecule) is reported in Figure 2b. The same band labeling adopted for I has been maintained for II to facilitate the comparison between them (A, 6.57 eV; B^I, 7.24 eV; B^{II}, 7.56 eV; B^{III}, 7.76 eV; B^{IV}, 8.33 eV; C, 9.5 eV). However, care must be taken in the interpretation because of the possibility of a different geometrical arrangement in vapor phase. Since we have not carried out any explicit calculation on II, we discuss its PE data qualitatively on an purely empirical basis.

No doubt exists in relating band A to the ionization from the half-filled HOMO; the intensity reduction and the IE shift toward lower values on passing from the PE spectrum of I to that of II are strongly diagnostic. Moreover, it is noteworthy that band B suffers a significant band envelope change and a shift toward lower IEs on going from I to II. The former effect demonstrates that the π^* NO and CO orbitals are significantly involved into the MOs giving rise to band B. The latter behavior can be interpreted as a metallic charge enrichment on replacing one NO by one CO, as expected on the basis of the aforementioned larger π acidity of NO.

Electrochemistry. $(\mu\text{-NO})_2[Co(Cp)]_2$ (I). The electrochemical reduction of I in DME–TBAB (0.2 M) at 25 °C occurs in a single two-electron irreversible and diffusion-controlled step. The profile of the RDLV wave (slope value of E vs. $\log (i_d - i)/i = 60$ mV) and the characteristics of the CV pattern (Figure 8), i.e., (a) shape of the cathodic peak ($E_{p/2} - E_p \simeq 50$ mV), (b) dependence of E_p on scan rate, V, (c) $i_p V^{-1/2}$ value independent of V in a wide range of scan rates, and (d) appearance of the coupled oxidation peak at far more anodic potentials ($\Delta E_p = E_p{}^a - E_p{}^c \simeq 700$ mV), suggest that the apparent irreversibility may conceal an ECE mechanism, i.e., two one-electron reductions separated by a chemical step with a Nerstian one-electron rate-determining step as the first electron transfer.

Exhaustive controlled potential electrolysis on the plateau of the wave requires 2 mol of electrons/mol of de-

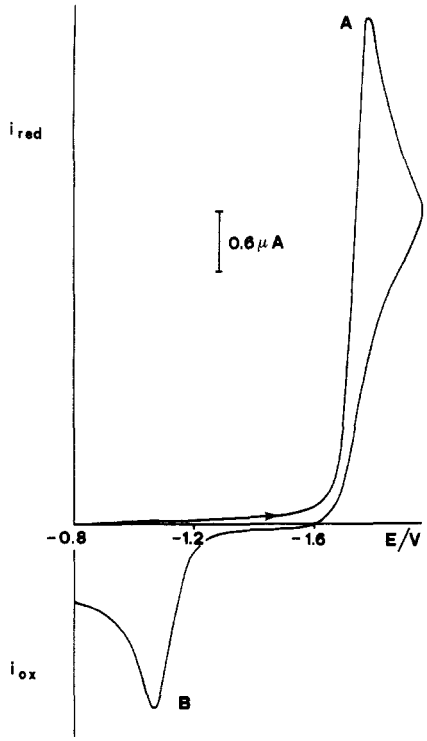

Figure 8. Cyclic voltammogram for reduction of 2.18 mM $(\mu\text{-NO})_2[Co(\eta^5\text{-}C_5H_5)]_2$ (I) in DME, 0.2 M TBAP, at 25 °C (scan rate, 200 mV s^{-1}).

polarizer and leads to a quite stable reddish solution with a voltammetric oxidation profile corresponding to the reduction pattern of the precursor. Indeed, a CV beginning in the reduction region exhibits an irreversible, two-electron oxidation corresponding to peak B in Figure 8. Reversal of this scan results in the detection of I by the linked reduction peak A, indicating that the overall reduction–oxidation process is chemically reversible. This was confirmed by the recovery of the starting compound upon subsequent reoxidation. The IR spectrum of the final catholyte displays a single nitrosyl absorption at 1570 cm^{-1}, a frequency intermediate between those of the neutral parent at 1585 and 1541 cm^{-1} and indicative of a terminal nitrosyl moiety in a highly reduced compound. The strong similarity between this spectrum and that exhibited by the sodium salt of III in acetonitrile[8] substantiates the assignment of the reduction product as III.

Hence, it appears that I undergoes scission upon electron addition

$$[CoCp(NO)]_2 + 2e^- \rightarrow 2[Co(Cp)(NO)]^- \quad (1)$$

being, however, not clear the ultimate mechanism of the electron-transfer process. In particular, an unambigous answer to the question as to whether the dianion resulting from the transfer of two electrons or the radical anion from one-electron transfer is the species that undergoes bridge splitting is lacking. As a matter of fact, the observed electrochemical pattern may be accounted for by the reaction sequence shown in (2)–(5) where the monomeric

$$[CoCp(NO)]_2 + e \leftrightarrow [CoCp(NO)]_2^{\bullet -} \quad (E_1°) \quad (2)$$

$$[CoCp(NO)]_2^{\bullet -} \rightarrow CoCp(NO)^{\bullet} + [CoCp(NO)]^- \quad (3)$$

$$CoCp(NO)^{\bullet} + e \leftrightarrow [CoCp(NO)]^- \quad (E_2°) \quad (4)$$

$$CoCp(NO)^{\bullet} + [CoCp(NO)]_2^{\bullet -} \rightarrow [CoCp(NO)]_2 + [CoCp(NO)]^- \quad (5)$$

species formed in the chemical reaction interposed between

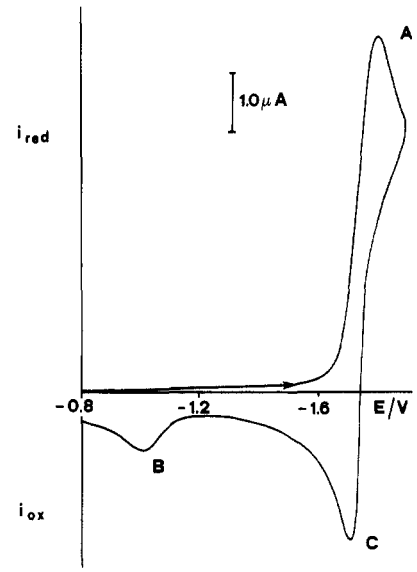

Figure 9. Cyclic voltammogram for reduction of 2.18 mM $(\mu\text{-NO})_2[Co(\eta^5\text{-}C_5H_5)]_2$ (I) in DME, 0.2 M TBAP, at −20 °C (scan rate, 4.0 V s^{-1}).

the two charge transfers (eq 3) is more readily reduced than the original dimeric compound (i.e., $E_2°$ anodic of $E_1°$), provided the rate of the chemical reaction is fast on the time window of the experiments.

CV tests carried out at lower temperatures (−20 °C) show the gradual transition from the starting two-electron reduction process to a one-electron cathodic response as revealed by the decrease of the $i_pV^{-1/2}$ value by about a factor of 2 as V is increased from 100 mV s^{-1} up to 10 V s^{-1}. The concomitant appearance and growing on the reverse scan of reversibly coupled anodic peak C (see Figure 9) attributable to the back-oxidation of fugitive $[CoCp(NO)]_2^{\bullet -}$ confirms the ECE character of the overall reduction process.

This allowed the kinetics of the reaction to be studied by chronoamperometry, a technique we considered more reliable than the CV one as it does not suffers from the degree of reversibility of the charge-transfer process. Thus, the rate constant value for the chemical step (3) was evaluated from the ratio of the observed current, i_k, to the diffusion-controlled current expected in the absence of the chemical complication, i_d, as a function of time, t, by means of eq 6.[22]

$$(2 - i_k/i_d) = \exp(-kt) \quad (6)$$

The data in Table III are for measurements carried out at −20 °C and times ranging from 1 to 500 ms. The excellent fit with the theory for a first-order reaction together with the observation that the values obtained in three independent determinations of the rate constant were independent, within a standard deviation of ±8%, of the substrate concentrations allows for any contribution from the electron-transfer reaction (5) to rate control to be ruled out and corroborates the proposed mechanism. Thus, the rate constant is found to be 4.4 (±8%) s^{-1} at −20 °C.

In line with this interpretation of the reduction pattern, it follows that the reoxidation of III back to I should proceed via a fast one-electron transfer generating a fugitive radical precursor, Co(Cp)(NO)•, followed by a dimerization pathway. Obviously, the confirmation of this latter inference awaited a detailed experimental analysis in order to test whether the CV oxidation pattern of III met the diagnostic criteria typical of a dimerization following the charge transfer.[23] Unfortunately, CV tests

Table III. Typical Determination of the Rate Constant for the Chemical Step in the Reduction of $(\mu\text{-NO})_2[Co(\eta^5\text{-}C_5H_5)]_2$ (I) in 1,2-Dimethoxyethane, 0.2 M TBAP, Solution at -20 °C[a]

t/s	i_k/μA	$i_k t^{1/2}/\mu$A s$^{1/2}$	$-\ln(2 - i_k t^{1/2}/i_d t^{1/2})$	k/s^{-1}
0.001	27.53	0.87_0[b]		
0.002	19.33	0.86_4[b]		
0.003	15.82	0.86_6[b]		
0.004	13.62	0.86_1[b]		
0.005	12.22	0.86_4[b]		
0.010	9.03	0.90_3	0.045	4.5
0.015	7.52	0.92_1	0.067	4.5
0.020	6.60	0.93_3	0.082	4.1
0.030	5.60	0.97_0	0.13	4.3
0.050	4.66	1.04	0.23	4.6
0.070	4.15	1.10	0.32	4.6
0.100	3.74	1.18	0.46	4.6
0.150	3.30	1.28	0.65	4.3
0.200	3.06	1.37	0.88	4.4
0.300	2.75	1.51	1.37	4.6
0.400	2.50	1.58	1.75	4.4
0.500	2.31	1.63	2.16	4.3

[a] Complex concentration = 2.42×10^{-3} M. [b] $i_d t^{1/2} = 0.86_5$ μA s$^{1/2}$.

performed on solutions of electrogenerated III have yielded no meaningful result. Indeed, attempts to detect the expected reduction peak reversibly linked to the oxidation signal of the depolarizer (see eq 4) were unsuccessful even at the lowest temperature (-30 °C) and at the fastest scan rate (10 V s^{-1}) explored, owing, probably, to a value of the rate constant for the dimerization pathway so high as to be out of reach of cyclic voltammetry. On the other hand, interferences by product adsorption on the electrode and/or by contamination of the electrode by decomposition products, because of which it was necessary to polish the electrode surface frequently during the experiments, caused broadening of the observed signal and prevented a detailed numerical analysis of the dependence of the peak potential on either scan rate or substrate concentration according to the quoted literature.[23]

As far as the oxidation of I is concerned, a representative cyclic voltammogram recorded at -20 °C is displayed in Figure 10. Under these conditions the complex appears to be oxidized in two subsequent uncomplicated one-electron reversible steps ($E_1° = -0.09_1$ V; $E_2° = 0.37_0$ V), as indicated by the usual parameters ($\Delta E_p \simeq 50$ mV; $i_a/i_c = 1$; constancy of E_p and $i_p V^{-1/2}$ with scan rate). Hence, our observations seem to parallel the previous ones described in ref 5 and confirm the existence of the redox series in eq 7.

$$[CoCp(NO)]_2 \overset{e}{\leftrightarrow} [CoCp(NO)]_2^{\bullet+} \overset{e}{\leftrightarrow} [CoCp(NO)]_2^{2+} \quad (7)$$

However, raising of the temperature produces a change in the voltammetric profile of the complex in that at 25 °C the cathodic peak coupled with the second oxidation process has completley disappeared for scan rates up to 200 mV s^{-1}, while the first oxidation process keeps its uncomplicated reversibility. This disappearance of the signal due to the reversible reduction of I^{2+} evinces tendency for the dicationic dimer to undergo nitrosyl bridge cleavage. This was confirmed by bulk electrolysis experiments. Exhaustive electrochemical oxidations of I at potentials on the second anodic wave at either 25 or -20 °C require two electrons/dimer and result in the formation of a brown product whose identity remains to be definitely established. We tentatively formulated it as $[CoCpS_X]^+$,

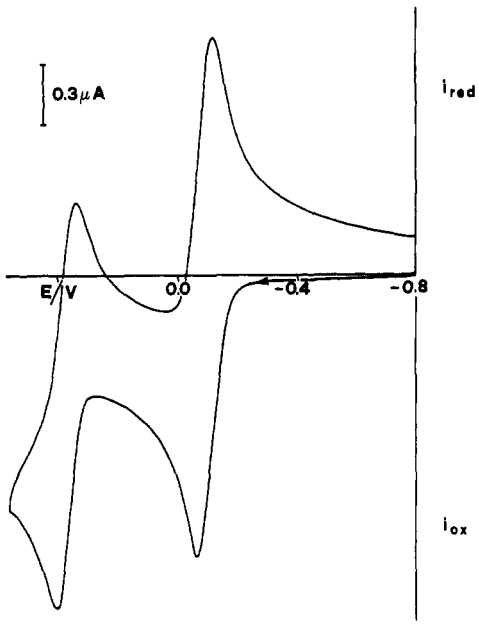

Figure 10. Cyclic voltammogram for oxidation of 2.18 mM $(\mu\text{-NO})_2[Co(\eta^5\text{-}C_5H_5)]_2$ (I) in DME, 0.2 M TBAP, at -20 °C (scan rate, 200 mV s^{-1}).

where S_X is a number of solvent molecules suitable for achieving coordinative saturation of the metal center, according to the following additional observations: (i) The IR spectrum of the final brown solution does not show any absorption in the M-NO region. (ii) Mass spectra examination of samples of the gases swept up during the electrolysis reveals the presence of NO in appreciable percentages. (iii) The polarogram at the dropping mercury electrode (the Pt microelectrode suffers from a deep passivation owing to coating with metallic cobalt) of the spent anolyte exhibits two reduction waves at $E_{1/2} = -1.33$ V (irreversible by mathematical analysis) and $E_{1/2} = -2.45$ V (highly reversible) with plateau currents in the ratio $h_1/h_2 \simeq 2$. Upon controlled potential electrolysis at a mercury pool on the plateau of the first wave one electron/Co atom is consumed as the solution changes from dark brown to purple and a black powder, afterwards identified as metallic cobalt precipitates. The presence in the final purple catholyte of $CoCp_2$ may be diagnosed from the identity of the voltammetric pattern (two redox couples centered at $E_1° = -1.36$ V and $E_2° = -2.45$ V) and UV-vis spectrum with those exhibited by an authentic sample of the cobalt complex generated in situ by the one-electron reduction of $[CoCp_2]^+$.[24] Quantitative analysis yields a value of 1 mol of $CoCp_2$ formed/mol of I in the original solution. Hence the polarographic picture would consist of reactions 8 and 9. (iv) Notably, the

$$2[CoCp]^+ + 2e \rightarrow CoCp_2 + Co \quad (8)$$

$$[CoCp_2]^+ \overset{e}{\leftrightarrow} CoCp_2 \overset{e}{\leftrightarrow} [CoCp_2]^- \quad (9)$$

intermediate formation of $[CoCp(CH_3CN)_3]^+$ has been claimed in the electrochemical oxidation of Co-polyolefin compounds in acetonitrile.[25] Hence, the dinitrosyl dication I^{2+} partecipates in chemical reactions in solution or decomposes as shown in eq 10.

$$[CoCp(NO)]_2^{2+} \rightarrow 2[CoCpS_X]^+ + 2NO \quad (10)$$

(23) Andrieux, C. P.; Nadjo, L.; Saveant, J. M. *J. Electroanal. Chem.* **1970**, *26*, 147.

(24) Geiger, W. E., Jr. *J. Am. Chem. Soc.* **1974**, *96*, 2632.
(25) Moraczewski, J.; Geiger, W. E. *Organometallics* **1982**, *1*, 1385.
(26) Granozzi, G.; Casarin, M., unpublished results.

However, all of the electrochemical and chemical data that would provide evidence in favor of the formation of the final oxidation product as $[CoCpS_X]^+$ may be alternatively accommodated on the basis of the formation from a CpCo-containing intermediate of $[CoCp_2]^+$, Co^{2+}, and Co according to the following interconversion

$$2[CoCp]^+ \rightarrow [CoCp_2]^+ + {}^1/_2Co^{2+} + {}^1/_2Co \quad (11)$$

In such a case, the first polarographic wave would be a composite of the two reduction processes $CoCp_2^{1+/0}$ and $Co^{2+/0}$. Indeed, the DME-solvated Co^{2+}, generated by anodic dissolution of metallic Co foil in DME/0.2 M TBAP, shows an irreversible wave with an $E_{1/2}$ value very close to the $E°$ value for the $CoCp_2^{1+/0}$ redox couple.

As far as the electrolysis at potential values corresponding to the first oxidation process is concerned, the final result at 25 °C is identical with that of the direct oxidation on the second peak: two electrons/dimer are removed to consume the reactant completely and the final electrolyzed solution exhibits spectral characteristics and polarographic profile virtually identical with those previously described. At low temperature (−20 °C), however, exhaustive electrolysis requires one electron/dimer and produces a dark mauve solution showing the voltammetric pattern of the neutral precursor, apart from a one-electron shift of the current scale, diagnostic of I^+. Its identity was substantiated by comparison of the IR (ν_{NO} = 1617 cm^{-1}), near-IR (λ_{max} = 535 and 990 nm), and ESR (15 lines) spectra with those of an authentic sample.[6] The subsequent one-electron oxidation at −20 °C results once again in NO evolution and concomitant formation of non-nitrosyl products (see above). Upon heating to 25 °C the solution turns gradually from mauve-red to a dark brown color with the contemporary flattening of every IR, vis, ESR, and voltammetric signal distinctive of the radical cation I^+. At the end of the conversion quantitative spectrofotometric and voltammetric analyses indicate that 0.5 mol of I and 1.0 mol of $[CoCpS_X]^+$ form for each mole of original I^+.

From these results it appears that the one-electron oxidation product of I, viz., I^+, is unstable in DME, unlike in CH_2Cl_2, and decays by a disproportionation pathway. Now, from the thermodynamic point of view, the instability of I^+ toward disproportionation is not predicted by its oxidation–reduction pattern in DME. Indeed, it appears that I^+ can both be reduced ($E_1°$) and oxidized ($E_2°$) in reversible steps, so that only the disproportionation equilibrium

$$2[CoCp(NO)]_2^{\bullet+} \leftrightarrow [CoCp(NO)]_2 + [CoCp(NO)]_2^{2+} \quad (12)$$

has to be taken into account. The hypothesis that the driving force for the disproportionation reaction is the high instability of I^{2+} that would promote a displacement of the equilibrium (12) far over to the right is in contrast with the well-established full stability of I^+, in spite of the short lifetime of I^{2+},[5] in CH_2Cl_2. In this context we tested by bulk electrolysis experiments in 1,2-dichloroethane that the ultimate fate of the transiently formed bimetallic dication is the same as in DME, i.e., release of NO and formation of CpCo-containing product.

Kinetic investigations carried out by either amperometric monitoring the reduction wave or IR monitoring the nitrosyl band of disappearing I^+ showed that the disproportionation reaction obeys first-order law and gave a rate constant of 8.5 (±0.5) × 10^{-4} s^{-1} at 25 °C. Hence, any contribution from eq 12 to rate control is ruled out; instead, nucleophilic attack at one Co atom of I^+ by the solvent, S, in the rate-determining step causing bridge splitting into

Table IV. Formal Reduction Potentials, $E°$, as a Mean Value ($E_p^a + E_p^c$)/2 of Cyclovoltammetry in 1,2-Dimethoxyethane, 0.2 M TBAP, vs. Ferricinium/Ferrocene Redox Couple (±3 mV) under Identical Experimental Conditions

redox couple	$E°$/V
$[CoCp(NO)]_2/[CoCp(NO)]_2^{\bullet-}$ (I^0/I^-)	-1.75_1
$[CoCp(NO)]_2^{\bullet+}/[CoCp(NO)]_2$ (I^+/I^0)	-0.09_1
$[CoCp(NO)]_2^{2+}/[CoCp(NO)]_2^{\bullet+}$ (I^{2+}/I^+)	0.37_0
$[CoCp_2(CO)(NO)]^{\bullet}/[Co_2Cp_2(CO)(NO)]^-$ (II^0/II^-)	-1.62_1
$[Co_2Cp_2(CO)(NO)^+/[Co_2Cp_2(CO)(NO)]^{\bullet}$ (II^+/II^0)	-0.01_1

CoCp(NO)• and $[CoCp(NO)S]^+$ followed by both the rapid dimerization of the monomeric radical (see above) and loss of NO from the spectroscopically undetectable, even transiently, solvated nitrosyl cation is strongly suggested (eq 13).

$$[CoCp(NO)]_2^{\bullet+} + S \xrightarrow{slow} CoCp(NO)^{\bullet} + [CoCp(NO)S]^+$$
$$\downarrow fast \qquad\qquad S \downarrow fast \quad (13)$$
$$^1/_2[CoCp(NO)]_2 \qquad [CoCpS_X]^+ + NO$$

Alternative to the dimerization reaction is the fast cross redox reaction (14), which may be important and should be considered as a possible pathway. Better nucleophiles,

$$CoCp(NO)^{\bullet} + [CoCp(NO)]_2^{\bullet+} \xrightarrow{S} [CoCp(NO)]_2 + [CoCp(NO)S]^+ \quad (14)$$

such as PPh_3 or Br^-, are considerably more effective in promoting the disproportionation reaction just as equimolar amounts of these species have been reported to convert instantaneously, even at low temperatures, I^+ into the neutral precursor and $[CoCp(NO)(PPh_3)]^+$[5] or CoCp(NO)Br,[6] respectively. Unlike the bromo and the phosphine derivatives, the DME-containing nitrosyl cation is unstable toward loss of NO as confirmed by the course of the reaction between CoCp(NO)Br and an equimolar amount of a halide abstractor, such as $AgClO_4$ and $TlClO_4$, in DME, which immediately results in the almost quantitative formation of NO and $[CoCpS_X]^+$.

As a consequence, the observed decomposition of the bimetallic dication in the coordinating solvent DME as well as in the noncoordinating one dichloroethane to NO and CoCp-containing species may be likely believed to proceed via spontaneous, probably solvent-assisted, symmetric splitting to give the solvated or unsolvated $[CoCp(NO)]^+$ intermediate whose ultimate fate is the release of NO and formation of non-nitrosyl organometallic products.

The formal potentials of the redox couples $[CoCp(NO)]_2^{0/1-}$, $[CoCp(NO)]_2^{1+/0}$, and $[CoCp(NO)]_2^{2+/1+}$ and the spectral characteristics of some binuclear Co complexes are collected in Tables IV and I, respectively.

(μ-NO)(μ-CO)[Co(η^5-C_5H_5)]$_2$ (II). Compound II is isoelectronic with I^+, so the two dimeric complexes would be expected to exhibit not substantially different behaviors. Indeed, the voltammetric pattern of II in DME at low temperature (−20 °C) consists of a single one-electron diffusion-controlled reduction step ($E°$ = -1.62_1 V) and of a single one-electron diffusion-controlled oxidation wave ($E°$ = -0.01_1 V). Both electrode reactions are essentially reversible, as shown by slope values of E vs. log $(i_d - i)/i$ plots for RDLV experiments and by differences in anodic/cathodic and cathodic/anodic peak potentials from CV experiments. Also, the ratios of direct to reversal peak currents are equal to unity and independent of sweep rate. At 25 °C, by analogy, the reduction process keeps its un-

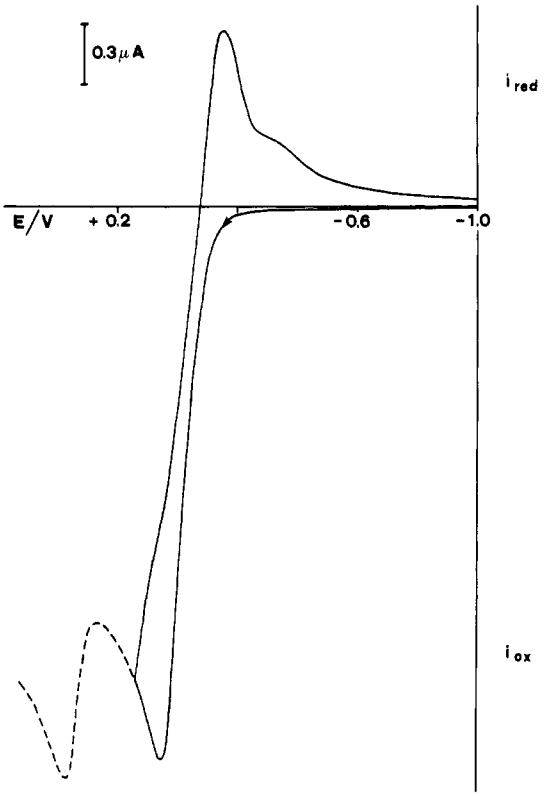

Figure 11. Cyclic voltammogram for oxidation of 1.90 mM (μ-CO)(μ-NO)[Co(η^5-C_5H_5)]$_2$ (II) in DME, 0.2 M TBAP, at 25 °C (scan rate, 200 mV s^{-1}).

complicated reversibility, and the CV oxidation profile, mimicing once again that found for I^+ under similar conditions, shows the disappearance of the reversibly coupled reduction peak as a proof of a follow-up chemical reaction after the electron transfer. The one significant difference is that the height of the oxidation peak of II corresponds, now, to passage of approximately 1.5 electrons, making it likely that the products of the chemical follow-up reaction also oxidized as they are formed at that potential. Reversal of the scan results in the detection of a cathodic peak at −0.12 V, which is attributed to I^+ as confirmed by the concomitant appearance on the voltammogram of the 0.37-V I^+ oxidation wave, when the scan is extended out to more positive values (Figure 11).

Potentiostatic reduction on the diffusion plateau of the cathodic wave of red II requires one electron/mole and leads to a stable green-brown solution whose voltammetric pattern is that expected for an uncomplicated reversible one-electron reduction. Formulation of the product as II^- is supported by the presence in the IR spectrum of the spent catholyte of a strong ν_{CO} band at 1735 cm^{-1} and a strong ν_{NO} absorption at 1436 cm^{-1}, approximately 100 cm^{-1} lower in energy than those of the neutral precursor (see Table I).

Exhaustive controlled potential electrolysis on the plateau of the oxidation wave at −20 °C results in the removal of one electron/dimer to yield 0.5 mol of I^+, 0.5 mol of $CoCp(CO)_2$, and 0.5 mol of $[CoCpS_X]^+$ for each mole of II as supported by voltammetric, IR, and polarographic measurements on the final anolyte, respectively. IR monitoring of the progress of the conversion verifies that the principal nitrosyl-containing product initially formed is I, which is more readily oxidized than II (see Table IV), thus converting with time into final I^+. GC–MS analysis of the stripped gas does not reveal any trace of NO.

If carried out at 25 °C, the electrolysis requires just the additional amount of charge expected for the two-electron oxidation of I via disproportionation of short-lived I^+ (see above) and the final organometallic products (in 1:3 ratio) are $CoCp(CO)_2$ and $[CoCpS_X]^+$.

Changing from DME to 1,2-dichloroethane as solvent does not alter the oxidation pathway of II. A one-electron oxidation, whatever the temperature, is observed, and the ultimate fate of the dimer is the same as in DME at −20 °C, i.e., formation of I^+, $CoCp(CO)_2$, and CoCp-containing species. However, the intermediate precursor II^+, likewise I^{2+}, is fairly long-lived in dichloroethane when compared with DME as inferred by the CV oxidation pattern of the parent dimer showing at 25 °C only incomplete chemical reversibility. As a matter of fact, the detection of II^+, mixed with $[CoCp(CO)(NO)]^+$ and $[Co_2Cp_2(CO)_2(\mu\text{-NO})]^+$, in the room-temperature reaction between $CoCp(CO)_2$ and $(NO)PF_6$ in CH_2Cl_2 has been previously reported.[4e,5] The overall stoichiometry of the reaction is given by eq 15.

$$2[Co_2Cp_2(CO)(NO)]^\bullet \rightarrow [CoCp(NO)]_2^{\bullet+} + CoCp(CO)_2 + [CoCp]^+ + 2e \quad (15)$$

The reaction may probably proceed via the sequential reactions 16–20, where the terms *fast* and *slow* refer to the cyclic voltammetry time scale and 25 °C. The electron-

$$[Co_2Cp_2(CO)(NO)]^\bullet \leftrightarrow [Co_2Cp_2(CO)(NO)]^+ + e \quad (16)$$

$$[Co_2Cp_2(CO)(NO)]^+ \xrightarrow{\text{fast}} [CoCp(CO)]^{\bullet+} + CoCp(NO)^\bullet \quad (17)$$

$$CoCp(NO)^\bullet \xrightarrow{\text{fast}} {}^1/_2[CoCp(NO)]_2 \quad (18)$$

$${}^1/_2[CoCp(NO)]_2 \leftrightarrow {}^1/_2[CoCp(NO)]_2^{\bullet+} + {}^1/_2e \quad (19)$$

$$[CoCp(CO)]^+ + [Co_2Cp_2(CO)(NO)]^\bullet \xrightarrow{\text{slow}} CoCp(CO)_2 + {}^1/_2[CoCp(NO)]_2 + [CoCp]^+ \quad (20)$$

transfer, ligand-transfer reaction (20) would account for the n = 1.5 value with detection of I^+ for the oxidation under the CV conditions and for the n = 1 value in the bulk coulometry experiments.

Finally, it is noteworthy that the *heterolytic splitting* of the intermediate into 15-electron $[CoCp(CO)]^{\bullet+}$ and 17-electron $CoCp(NO)^\bullet$(eq 17), unlike the *homolytic* reaction mode into 16-electron CoCp(CO) and $[CoCp(NO)]^+$, is found to properly rationalize this oxidation process, for cyclic voltammetry measurements, controlled potential coulometry, and bulk electrolysis product distribution are all found to be consistent with this way of cleavage.

The formal potential of redox couples $II^{0/1-}$ and $II^{1+/0}$ and the spectral characteristics of the II^Z series (z = 0, 1−) are collected in Tables IV and I, respectively.

Conclusions

As concluding remarks, we want to report here some comments on the electrochemical data based on the reported DV–Xα theoretical results.

A close relationship between the nature of the frontier MOs, as emerging from our calculations (see Figures 6 and 7), and the chemical transformations of I upon either removal or addition of electrons is evident. Actually, the preservation of the dimeric structure when one electron is removed, giving rise to I^+, is in tune with the Co–Co antibonding nature of the HOMO, to which the NO bridges contribute to a negligible extent. The removal of one electron from HOMO, however, implies the bent → planar interconversion, as found by X-ray structure determination of I^+ in the solid state and IR measurements in solution.[6] Similar considerations can be put forward to explain the stability of the reduction product of II

(isoelectronic with I), for which a bent structure should be forecast.

On the contrary, the addition of one electron into the LUMO, which is strongly Co–NO antibonding (see Figure 7), labilizes the Co–NO bonds, giving rise eventually to monomeric fragments.

Removal of a further electron from I^+ should not affect the dimeric structure. Interestingly, I^{2+} is detected only as a short-lived species whose fate is fragmentation with loss of NO. An explicit calculation on I^{2+} demonstrates that the reason for such a behavior is an extensive weakening of the $d_\pi(Co) \rightarrow \pi^*(NO)$ back-donation interactions owing to the high positive charge on the metal atoms.[26] This argument, however, cannot be invoked to explain the instability of II^+. We could tentatively attribute the mentioned *heterolytic splitting* of II^+ to the inherent molecular asymmetry consequent to the presence of two different bridging groups that would induce some destructive charge polarization upon oxidation.

A final comment on the Co–Co interaction in these dimers is of relevance. At the present level of theoretical accuracy we can assess that a direct metal–metal interaction is present only when I assumes a bent geometry. This and other minor factors, such as the reduction of the Co–Cp antibonding interaction which stabilizes the HOMO in the bent form, contribute to the bending of the $(\mu\text{-}NO)_2Co_2$ core which, however, occurs to the prejudice of the Co–NO interactions (Co–NO overlap populations, planar, 0.96 e, and bent, 0.83 e). The final geometry is, then, the result of a subtle balance between small perturbations (e.g., crystal packing energies).[16]

Acknowledgment. We thank the Ministero della Pubblica Istruzione for financial support to this study and Mr. S. Sitran of IPELP (CNR) for technical assistance.

Registry No. I, 51862-20-5; I^{2+}, 68813-15-0; I^+, 68875-56-9; II, 58071-48-0; II^+, 103259-02-5; II^-, 106212-33-3; III, 64236-02-8; Co, 7440-48-4.

Hydroformylation of Formaldehyde with the $[Rh(CO)_2Cl_2]^-$ and $[Rh_5(CO)_{15-x}(PPh_3)_x]^-$ System: A Case of Synergetic Catalysis with Two Combined Rhodium Carbonyl Species in Different Oxidation States

Mario Marchionna and Giuliano Longoni*

Dipartimento di Chimica Inorganica e Metallorganica e Centro del CNR per lo Studio della Sintesi e della Struttura, 20133 Milano, Italy

Received June 26, 1986

Paraformaldehyde has been hydroformylated to glycolaldehyde at 100–140 atm of CO and H_2 (1/1) and at 90–110 °C with selectivity up to 95% in common organic solvents, e.g., acetone, with a catalytic system involving two preformed anionic rhodium carbonyl species in different formal oxidation states, viz., $[Rh(CO)_2Cl_2]^-$ and $[Rh_5(CO)_{15-x}(PPh_3)_x]^-$. This system combines the high activity of the latter with the high selectivity of the former and enables the hydroformylation of paraformaldehyde to be carried out at a rate comparable with that previously observed only in N,N-disubstituted amide or pyridine solvents. A strictly related system, generated "in situ" upon addition of halide ions and triphenylphosphine to $Rh_4(CO)_{12}$, showed comparable catalytic behavior. A temptative interpretation of the synergetic effect shown by mixtures of $[Rh(CO)_2Cl_2]^-$ and $[Rh_5(CO)_{15-x}(PPh_3)_x]^-$ is suggested.

Introduction

Glycolaldehyde from hydroformylation of formaldehyde is receiving increasingly wider attention as a potential intermediate for ethylene glycol and serine production.[1-5] So far the metal-catalyzed hydroformylation of formaldehyde to glycolaldehyde has been achieved with reasonable rates and high selectivity only with Rh(I) phosphine–carbonyl complexes either in ionizing and basic solvents, e.g., N,N-disubstituted amides[2,3] or pyridines,[4] or in the presence of weak organic bases as promoters, e.g., triethylamine.[3,4]

Also when $Rh_4(CO)_{12}$ was used as catalyst precursor, in the presence of PPh_3 and HI as promoters, a highly selective hydroformylation of paraformaldehyde to glycolaldehyde was only observed in basic solvents such as dimethylformamide (DMF).[6] Concomitant gas chromatographic analyses and infrared measurements suggested the possible involvement of the $[Rh_5(CO)_{15-x}(PPh_3)_x]^-$ (x = 1, 2)[7] substituted carbonyl cluster in the catalytic system.[6] Therefore, in keeping with previous suggestions,[3] it appeared conceivable that one role of such ionizing and basic solvents was to enable reduction of oxidized rhodium precursors to low-valent anionic rhodium carbonyl species. However, at partial difference with previously investigated systems,[3] both preformed $[Rh_5(CO)_{15-x}(PPh_3)_x]^-$ (x = 0, 1) species and $Rh_4(CO)_{12}/PPh_3/HI$ mixtures in DMF displayed progressive loss of selectivity with time, apparently corresponding with a further reduction to lower valent species of the precursors.[6,8] It was, therefore, of interest

(1) Hendriksen, D. E. *Chem. Eng. News* **1983**, April 11, 41–42.
(2) Spencer, A. *J. Organomet. Chem.* **1980**, *194*, 113–123.
(3) Chan, A. S. C.; Carroll, W. E.; Willis, D. E. *J. Mol. Catal.* **1983**, *19*, 377–391 and references therein.
(4) Okano, T.; Makino, M.; Konishi, H.; Kiji, J. *Chem. Lett. Jpn.* **1985**, 1793–1796.
(5) Kaneko, T. *Synthetic Production and Utilization of Amino Acids*; Wiley: New York, 1974 and references therein.
(6) Marchionna, M.; Longoni, G. *Gazz. Chim. Ital.* **1986**, *116*, 453–457.
(7) Martinengo, S.; Fumagalli, A.; Ciani, G.; Sironi, A., unpublished results.
(8) Marchionna, M.; Longoni, G. *J. Mol. Catal.* **1986**, *35*, 107–118.

0276-7333/87/2306-0606$01.50/0